Nanostructured fumarate copolymer-chitosan crosslinked scaffold: an in vitro osteochondrogenesis regeneration study

Lastra, María Laura[1,2]; Molinuevo, María Silvina[1*]; Blaszczyk-Lezak, Iwona[3]; Mijangos Carmen[3]; Cortizo, María Susana[2*]

1 Laboratorio de Investigación en Osteopatías y Metabolismo Mineral (LIOMM). Facultad de Ciencias Exactas, UNLP (1900), 47 y 115, La Plata, Argentina.

2 Instituto de Investigaciones Fisicoquímicas Teóricas y Aplicadas (INIFTA), CCT-La Plata, CC16 suc. 4 (1900) La Plata, Argentina.

3 Instituto de Ciencia y Tecnología de Polímeros, CSIC, Juan de la Cierva 3, 28006 Madrid, España.

*Corresponding authors:

Molinuevo, María Silvina

Laboratorio de Investigación en Osteopatías y Metabolismo Mineral (LIOMM). Facultad de Ciencias Exactas, UNLP (1900), 47 y 115, La Plata, Argentina. E-mail: silvinamolinuevo@yahoo.com.ar

Cortizo, María Susana

Instituto de Investigaciones Fisicoquímicas Teóricas y Aplicadas (INIFTA), CCT-La Plata, CC16 suc. 4 (1900) La Plata, Argentina. E-mail: gcortizo@inifta.unlp.edu.ar

This article has been accepted for publication and undergone full peer review but has not been through the copyediting, typesetting, pagination and proofreading process which may lead to differences between this version and the Version of Record. Please cite this article as an 'Accepted Article', doi: 10.1002/jbm.a.36260

Abstract

In the tissue engineering field the design of the scaffold inspired on the natural occurring tissue is of vital importance. Ideally, the scaffold surface must promote cell growth and differentiation, while promote angiogenesis in the in vivo implant of the scaffold. On the other hand, the material selection must be biocompatible and the degradation times should meet tissue reparation times. In the present work, we developed a nanofibrous scaffold based on chitosan crosslinked with diisopropylfumarate-vinyl acetate copolymer using anodized aluminum oxide (AAO) templates. We have previously demonstrated its biocompatibility properties with low cytotoxicity and proper degradation times. Now, we extended our studies to demonstrate that it can be successfully nanostructured using the AAO templates methodology, obtaining a nanorod-like scaffold with a diameter comparable to those of collagen fibers of the bone matrix (170 and 300 nm). The nanorods obtained presented a very homogeneous pattern in diameter and length, and supports cell attachment and growth. We also found that both osteoblastic and chondroblastic matrix production were promoted on bone marrow progenitor cells and primary condrocytes growing on the scaffolds, respectively. In addition, the nanostructured scaffold presented no cytotoxicity as it was evaluated using a model of macrophages on culture.

Keywords: Nanostructured Biomaterials; Bone regeneration; Cartilage regeneration; Polyfumarate; Chitosan.

1. Introduction

In the recent years, it has been recognized the role that play the mimicry of the extracellular matrix in the tissue engineering field. It is supposed that when a scaffold is more similar to the specific extracellular matrix of a tissue better tissue integration and reparation was achieved. In this sense, it has been highlighted the importance both of the chemical nature and the micro- or nano-structuration of the scaffold surfaces to improve cell adhesion and growth [1]. The design and fabrication of bioinspired nanomaterials for tissue engineering applications requires a fundamental understanding of the interactions between polymers, nanostructures and cells [2]. In particular, in bone tissue engineering the organic proteins extracellular matrix is composed mainly by collagen fibers with a diameter between 50 to 500 nm. These nanofibers act as a natural scaffold over which osteoblastic cell development and maturation occurs. The development of scaffolds of dimensions similar to these fibers could promote the development of bone tissue.

Nanotechnology has emerged as a powerful technology in applied biomedical sciences. Polymeric nanofibers can be obtained by different methodologies and processing techniques [3-6]. Between them, template-based methods facilitate the fabrication of scaffolds in the nano-size with very well defined high aspect ratio and very good reproducibility [6]. The wetting of porous anodized aluminum oxide templates (AAO) with polymer-containing mixtures is a simple and versatile method for the nanostructuration of materials into tubular structures with diameters ranging from a few tens of nanometers to micrometers.

Nanostructured biomaterials mimic the extracellular matrix providing a better environment for cells to grow and survive; in consequence the nano-rough materials could also improve cell-biomaterial interactions when compared to macro-rough scaffolds [4, 7-8]. It

has been suggested that nanofibrous scaffolds presented an interconnected porous structure which provides a large surface area for cell attachment and sufficient space for nutrient exchange as well as angiogenesis [4]. Moreover, some authors found that scaffolds nanostructured improve cellular biocompatibility, increasing cell development and differentiation and wound healing while decreasing inflammatory properties [9-11].

Concerning materials of which scaffolds are made of, polymer blending and crosslinking are one of the most effective approaches for providing new, desirable polymeric materials for particular applications. In this sense, we have previously designed and characterized a fumaric copolymer crosslinked with chitosan [12]. In that work, we demonstrated that the scaffold obtained promote osteo- and chondrogenic development, with very low inflammatory response and an adequate degradation rate to promote osteochondral tissue reparation. In the present work, we have developed nanostructured scaffold based on a copolymer of chitosan and polydiisopropyl fumarate (PFVH-CH-B) using AAO. In addition, we have study the osteochondral biocompatibility and potential cytotoxicity of this material to be used in tissue engineering.

2. Materials and methods

2.1. Materials

Chitosan (CH, Sigma-Aldrich, high molecular weight), Borax (Timper Laboratorios, 99.9%), Methanol (99.9%, Aldrich), Chloroform (Scharlau), Acetic acid (Scharlau), hydrochloric acid (37%, Anhedra RA), and $CuCl_2$ (97%, Aldrich) were used as received without further purification. Ultrapure (99.999%) aluminum foils of 12 cm^2 were purchased

from Goodfellow and degreased by sonication into solvents of different polarity (acetone, deionized water and ethanol).

2.2. Synthesis anodic aluminum oxide templates

Three types of anodized aluminum oxide templates (AAO) were prepared with different pore dimensions, via a two-step electrochemical anodization process on Aluminum sheets, as it was previously described [13]. The resulting template presented an anodic aluminum oxide top layer with pores of around 170 nm in diameter and 750 nm of length arranged into a hexagonal lattice (AAO170), and a non-oxidized Al layer substrate at its bottom. Treating these templates with phosphoric acid (5 wt% at 35 ºC) during 60 min was obtained a second type of templates with a pore size of 300 nm (AAO_{300}) [14-15]. Moreover, using the same method [13], we also obtained a third template of 30 μm of length and 170 nm in diameter of pore (AAO^{30L}). The obtained AAO templates were annealed at 150 ºC in vacuum in order to remove the possible adsorbed organic molecules from the pore walls. After, the AAO templates were characterized by Scanning Electron Microscopy (SEM), FESEM Hitachi model SU8000 microscope. The figure 1 shows the structure of the templates of 750 nm of length of pore (3D image, A) before (B) and after (C) phosphoric acid treatment. The analysis of the images showed that the templates presented nano-porous highly regular on size and diameter. The nanocavities are homogeneous in its length (Fig. 1A), and its pore diameter was 170 nm (Fig 1B, AAO_{170}) or 300 nm (Fig 1B, after phosphoric acid treatment, AAO_{300}).

2.3. Preparation and characterization of the PFVH and chitosan composite biomaterial

First, diisopropylfumarate (DIPF)-vinyl acetate (VA) copolymer was synthesized by mass radical polymerization, hydrolyzed and characterized following a procedure previously described [12]. Briefly, both monomers (DIPF:VA, 75:25) together with the previously weighed mass of the initiator (40 mM) were charged into a reaction vessel and then purged with N_2 during 30 min. Reaction vessels were irradiated at 140 W during 25 min using a microwave oven (Zenith, ZVP-2819) of 2 450 MHz microwave frequency and 700 W maximum power. After reaching room temperature, the copolymer was isolated by hexane addition, purified by solubilization–precipitation (chloroform:hexane, 1:7), and then dried at constant weight for conversion estimation. The copolymer was named PFV. In order to introduce a hydroxyl group to the main macromolecular chain, PFV was submitted to basic hydrolysis. To this end, the copolymer was suspended in methanol (15% wt/v) and 1% wt/v NaOH solution was added (50 ml NaOH/15 g copolymer); then the solution was stirred at 50 °C for 1 h. After the reaction, the methanol was evaporated under vacuum, and the resulting solid was washed with water and dried until constant weight. Scheme 1 shows the chemical structure of the copolymer synthesized designated PFVH.

To obtain the composite biomaterial, a mixture of 50% w/w chitosan (CH) and the previously synthesized copolymer were cross-linked *in situ* with borax. The obtained sample was casted by evaporating the solvent (acetic acid) at room temperature on Teflon molds. This mixture was designated as PFVH-CH-B. The maximum swelling and water absorption capacity of the scaffolds were determined as it was previously reported [12].

In order to thermally characterize the material obtained, the glass transition temperature (T_g), PFVH-CH (mixture without borax) and PFVH-CH-B, were determined by Differential Scanning Calorimetry (DSC) (DSC 8500 with Hyper DSC-Perkin Elmer) under a nitrogen atmosphere. In brief, samples were placed in covered aluminum pans and then

placed in the DSC sample holder. Thermal cycles consisted of a heating ramp, followed by a cooling ramp, and a final heating ramp, using processes of heating and cooling of 10 ºC/min from -20 ºC to 200 ºC. Also, the thermal stability of PFVH-CH and PFVH-CH-B was analyzed by Thermogravimetric analysis (TGA) (TGA Q500-TA Instruments) under nitrogen atmosphere, gas purge at 90 mL/min, and ramp from room temperature to 700 ºC.

2.4. Biomaterial nanostructuration and characterization

The nanostructured scaffolds (NS) were prepared by infiltration of PFVH-CH-B into the AAO nanocavities by the melt precursor film - wetting method [13]. For the infiltration procedure, the copolymer film was placed on the AAO_{170} and AAO_{300} template surfaces and then infiltrated in an oven at 140 °C (higher temperature than the Tg of copolymer), under nitrogen atmosphere during 6 h [16]. During this process, the copolymer was pressed over the template every 15 min to promote infiltration. For the template of 30 μm of length of pore (AAO^{30L}) the infiltration conditions used were 140 °C under nitrogen atmosphere during 18 h. At the end of the infiltration process, the excess of copolymer was removed from the top surface of AAO template with a sharp blade. Following this methodology three nanostructured scaffolds were obtained NS170, NS300 and NS30L using $AAO_{170,}$ AAO_{300} or AAO^{30L} templates, respectively.

The AAO templates and all the infiltrated samples were morphologically characterized by SEM. In order to perform the analysis of free copolymer nanofibers the aluminum substrate was eliminated by treatment with a mixture of HCl, $CuCl_2$ and H_2O. Then, the alumina was dissolved in 10 wt% H_3PO_4 over night at room temperature. Previously, in order to support the free nanostructures, a polymethyl methacrylate coating

was placed over the template, that has been seen does not interfere with future determinations [17-18].

In order to see the effect of infiltration of copolymer distribution in AAO, Raman measurements were carried out using a Renishaw In Via Reflex Raman system with an optical microscope coupled to the system. The Raman scattering is excited using a diode laser at a wavelength of 785 nm. The laser beam is focused on the sample with a 0.85 x 100 microscope objective. The laser power at the sample, the exposure time and number of accumulations for the Raman measurements correspond to 320 mW, 10 seconds and 10 scans, respectively. PFVH-CH-B infiltrated into AAO templates of 30 μm of length and PFVH, CH, PFVH-CH-B, were studied by Raman spectroscopy at room temperature. Depth profiles were obtained by focusing the microscope stepwise, at 5 μm intervals, through the AAO template. The samples were measured in the 3 500–300 cm^{-1} spectral range.

Water contact angles (WCA) were measured in NS170 and NS300 using a KSV Theta goniometer at room temperature. Double-distilled water was placed on the air facing surfaces of the samples and a charge coupled device camera was used to capture the images of the water droplets for the determination of the contact angles. At least six measurements on different positions on the sample surface were performed to calculate the mean static contact angle.

2.5. Biocompatibility assay

2.5.1. Cell cultures and incubations

For biocompatibility assays bone marrow progenitor (BMPC) and chondrocyte cells were used. BMPC were isolated from the femora of Sprague-Dawley rats and cultured according to Molinuevo et al. [19]. Cells were maintained in basal media (DMEM-10 % FBS)

at 37 ºC. Cell adhesion and proliferation was evaluated by the MTT assay. This assay measures the reduction of the tetrazolium salt 3-(4,5-dimethylthiazol-2-yl)-2,5-diphenyl tetrazolium bromide (MTT) to formazan by intact mitochondria in living cells. Thus, absorbance change is directly proportional to the number of viable cells. Briefly, 2.5 x 10^4 cells / well in basal media were plated onto the scaffolds which were casted on multiwell culture plates and cultured during 2 h (adhesion), 24 h and 72 h (proliferation). After these culture periods, cells were incubated for two additional hours with a solution of 0.1 mg/ml MTT. After washing, the formazan precipitate was dissolved in DMSO and the absorbance read at 570 nm.

Alternatively, chondrocytes were isolated from the xiphoid process of the sternum of Sprague-Dawley adult rats after dissection of the perichondrium. Briefly, the cartilage was minced, washed three times in phosphate saline buffer pH 7.4 (PBS) and treated with trypsin for 15 min at 37 °C. After that cartilage was washed three times with DMEM-10% FBS and maintained in culture at 37 °C under 95% air and 5% CO_2 with half of the culture media changed every three days [20]. After 15 days, chondrocytes outgrowths from the cartilage were replated on the scaffolds and the differentiation assay was conducted as described above.

All procedures were in accordance with the Guide for the Care and Use of Laboratory Animals published by the National Institutes of Health, and they were approved by the Institutional Laboratory Animal Care and Use Committee (CICUAL Protocol Number 019-06-15, Facultad de Ciencias Exactas, UNLP).

2.5.2. Osteoblastic differentiation

The effect of the material properties (nanostructuration) on the osteogenic commitment was evaluated by growing BMPC on the scaffolds during 21 days and then the

activity of alkaline phosphatase, production of type I collagen, and mineral deposition was

Additionally, osteogenic induction of BMPC was performed by incubating the cells in basal media plus β-glycerol-phosphate and ascorbic acid during different periods of time: 15 and 21 days. After that time points type I collagen was evaluated through the colorimetric assay with Sirius red and alkaline phosphatase activity by the conversion of p-nitrophenyl phosphate to p-nitrophenol in a glycine buffer pH 10, and mineral deposits were analyzed with the colorimetric assays of Alizarin S red [12].

2.5.3. Chondroblastic assays

To evaluate the cartilage extracellular matrix produced by chondrocytes we determined the proteoglycans deposits after 15 days by the colorimetric method using alcian blue pH 2.5. Briefly, cells were fixed with formalin during 15 min and stained overnight with alcian blue. After washing, the stained material was distained with 1ml of dimethyl sulfoxide (DMSO). The absorbance was determined at 600 nm.

2.5.4. Evaluation of cytotoxicity

To determinate the eventual cytotoxicity of the biomaterial we evaluated the production of nitric oxide (NO) and interleukin-1β (IL1β) using a model of macrophages in culture. Briefly, RAW264.7 macrophages were grown on the scaffolds or the tissue culture plates (control condition) in DMEM without phenol red 5% FBS. After 6, 48 and 72 h the supernatants were collected and evaluated for NO production by the Griess' assay. IL1β production was evaluated by ELISA kits (BD OptEIA™ mouse IL-1β ELISA) in the conditioned media 24, 48 and 72 h of incubation. Alternatively, for PCR studies total RNA was isolated from cultured RAW264.7 after 72 h by the TRIZOL reagent method as

suggested by the manufacturer (Invitrogen, Argentina). The RNA expression of citotoxicity markers (IL1β, tumor necrosis factor α (TNFα) and Nitric oxide synthase (iNOS)) were analyzed using the semi-quantitative reverse transcription–polymerase chain reaction (PCR) using MMLV-RT (Invitrogen, Argentina). All the markers were normalized using actin as housekeeping. The specific primers for the markers were designed from NCBI sequence data, using CLC Genomics Workbench software (QIAGEN) (Table 1) and band intensity was quantified using the gels plug-in of MBF ImageJ program.

Additionally, the effect of the degradation products of the biomaterials on cell viability was also evaluated. Briefly, the scaffolds were incubated in DMEM at 37°C during 2 weeks. After this the supernatants (conditioned media) were exposed to the monolayer of BMPC during 24 and 72h. Thereafter, the MTT assay was performed as it was described above.

2.6. Statistical analysis

Results are expressed as the mean ± SEM and, unless indicated otherwise, were obtained from two separate experiments performed in triplicate. Differences between groups were assessed by one-way ANOVA with Tukey post hoc test. For non-Normal distributed data non-parametrical Kruskal–Wallis with Dunn's post hoc test was performed, using Graph Pad InStat v. 3.00 (Graph Pad Software, San Diego, CA, USA). $p< 0.05$ was considered significant for all statistical analyses.

3. Results and Discussion

3.1. AAO Templates

As described in the experimental section, AAO templates were synthesized by a two-step electrochemical anodization process to yield well defined porous nanocavities. Figure 1 presents the SEM images of the templates. The characteristic dimensions of the templates synthesized are given in Table 2: AAO_{170} and AAO_{300} represent the templates of 750 nm of length with 170 nm and 300 nm in diameter, respectively. While AAO^{30L} represent the template of 30 μm of length and 170 nm in diameter.

3.2. Characterization of the PFVH-CH and PFVH-CH-B

The swelling behavior of PFVH-CH and PFVH-CH-B were compared in PBS buffer at 37 ^{o}C. Both samples maintained its structural integrity up to the maximum time tested (90 min) and they showed a similar behavior as a function of time, reaching the equilibrium within 30 min. However, the maximum swelling attained was different: 300 ± 13 % and 180 ± 7 % for PFVH-CH-B and PFVH-CH, respectively. Since the proportion of PFVH and CH was the same in both materials, the highest swelling attained by the cross-linked material could be assigned to the inclusion of the ionic crosslinker (borax).

On the other hand, one important condition for the use of the infiltration method in AAO templates by wetting method is that the polymeric material must be infiltrated above its Tg and therefore needs to be thermally stable. In order to evaluate this characteristic of our materials, DSC and TGA measurements were carried out.

DSC measurements for PFVH-CH with and without borax showed a glass transition temperature (Tg) of 64.8 ºC and 62.15 ºC, respectively. Moreover, these values are higher than those previously found for PFVH (Tg = 60.5 ºC) [12]. The increase on Tg of PFVH-CH-cross linked by borax could be attributed to the restriction on the catenary movements caused

by the crosslinking between both polymers with borax. A similar behavior was previously observed for other systems [21].

The thermal stability of materials was assessed by TGA under nitrogen atmosphere; Table 3 shows the results obtained. PFVH-CH and PFVH-CH-B materials seemed to thermally decompose in three steps and showed high initial decomposition temperatures (IDT), although highest for non-cross-linked material. The two first decomposition events (T_1 and T_2) could be attributed to the copolymer degradation, as it was previously observed for other fumaric copolymers [22]. The last thermal event, at T_3, shows the complete degradation of the macromolecular structure. As it can be observed in Table 3, cross-linked material (PFVH-CH-B) exhibited a higher T_3 with lesser total mass loss compared to PFVH-CH. These results demonstrate the higher thermal stability of the cross-linked material compared to non-cross-linked one. Similar results were observed for other system based on cross-linked polysaccharides [23] [24]. Thus, these results indicate that our material could be satisfactorily nanostructured using AAO templates at 140 °C without degradation thereof.

3.3. Infiltration of PFVH-CH-B and characterization of the nanofibers

PFVH-CH-B nanofiber-structured scaffolds have been prepared as described in experimental section and they have been cut into small pieces to perform macro and microscopic morphological studies. The macroscopic appearance of the membrane is presented in Figure 2A. In this image it can be observed that the nanostructured scaffolds (NS170 and NS300) were more transparent than CS and NS30L membranes. This difference it is probably caused by the higher mass presented on CS and NSL30. The morphological studies through scanning electronic microscopy (SEM) allow us to examine the copolymer nanofibers (after demolding) to evaluate its length, diameter and distribution obtained

(Figure 2B-E). In a lateral view illustrating the length of the fibers, we found that the short nanofibers (NS170 and NS300) presented a homogeneous distribution in length and in the spaces between them (Figure 2B). While NS30L nanofibers give rise to a disordered scaffold where the fibrous structure are collapsed and nanorods showed a bunche-like condensed structure (Figure 2C). In figures 2D and 2E it can be observed the top view of the extracted PFVH-CH-B copolymers from AAO templates of 750 nm of length with 170 nm and 300 nm of diameter, respectively. From these figures it can be seen that nanofibers diameters were very homogeneous and coincident with those of the template, showing that the copolymer completely filled the nanocavities.

We also evaluated the presence of copolymers along the length of nanocavity by Raman spectroscopy. First we evaluated Raman spectra of chitosan, PFVH and PFVH-CH-B (Figure 3A). Chitosan showed bands at 2 880 cm^{-1} that corresponds to the ν(C-H) stretching vibration of the pyranoid ring, and others at 1 376, 1 260 and 896 cm^{-1} which could be assigned to $\delta(CH_3,CH_2)$ bending vibrations, ν(C-O) stretching vibration and ν(C-C) pyranoid ring stretching-vibration, respectively [25]. PFVH presented characteristic bands at 1 732 and 829 cm^{-1} that corresponds to the ν(C=O) and $\nu(C\text{-}CH_3)$ stretching vibration, respectively. The PFVH-CH-B Raman spectra exhibited the characteristic bands of both components.

Figure 3B shows the Raman spectra depth of PFVH-CH-B with pinhole taken at different intervals. Despite the noise due to the fluorescence of the alumina, it was possible to observe all the characteristic bands previously indicated in the Raman spectra depth up to 25 μm, which demonstrate that no changes in chemical composition by degradation or other chemical or physical process are observed. As it has been reported, the decrease in the intensity of the bands with the depth of the cavity can be only attributed to the decrease in the transparency of the sample with the profundity [26].

Some results have indicated that certain cell lines are strongly affected by artificially fabricated micro or nano-structured solid surfaces, and implied that is possible to control the cell behaviors in vitro by using surface topologies instead of chemical or biological reagents [27]. So, WCA measurements (related to the polarity of the material) have been undertaken in order to investigate and understand, if any, the effect of nanostructuring the material on cell adhesion/proliferation.

The measure of the WCA showed that the PFVH-CH-B nanostructured scaffolds present lower values than that observed for casted scaffold (CS), indicating the increasing of hydrophilicity by nanostructuring (Table 4). In addition, we found a lower value of contact angle for the matrix with smallest diameter fibers (NS170).

Based on the WCA measurement, it has been explained the behavior of wetting of solids with porous or textured architecture by different models [28-29]. These models consider the effect of the roughness factor (r) and the area fraction of the solid surface (ϕ_s) in contact with the water drop. It has been demonstrated that the contact angle will increase with increased roughness of a hydrophobic surface, whereas the contact angle will decrease with increased roughness of a hydrophilic surface. The results of our scaffolds exhibited a behavior more close to hydrophilic surface, although the WCA of CS is 103°> 90°, while both NS surfaces showed lower values of WCA than the casted scaffold (CS). On the other hand, the lower value for NS170 in comparison to NS300 could be correlated with the increase of the smooth zone between the nano-pillars which promotes a higher wet surface (evaluated as the distance between pillars, d, Table 4) and therefore a decrease in the apparent contact angle (greater hydrophilicity), according to the Wenzel model. Similar behavior caused by nanostructuration has been previously reported [30]. Based on these results,

we proposed that the nanostructured scaffolds would promote cellular growth and development.

3.4. Biocompatibility assays

For biocompatibility studies, we select two nanostructured scaffolds (NS170 and NS300) in order to evaluate possible differences on biological response caused by the diameter of the nanorods. Previous experiments demonstrated that the scaffolds with ordered structures promote osteoblastic differentiation compared with non-ordered structures, as is the case for NS30L [5, 10-11]. Therefore the biocompatibility studies were carried out for the shorter length nanostructures, NS170 and NS300.

In a first set of experiments, we evaluated the adhesion of bone marrow progenitor cells on the nanostructured scaffolds compared to tissue culture surfaces after 2 h of plating by the MTT assay. We found that BMPC adhered better to the tissue culture dishes surface (plastic) than to the scaffolds (Figure 4A, white bars). However, growth rate was equivalent on the plastic and the nanostructured surfaces (Figure 4A). We have previously demonstrated that BMPC growth was equivalent on tissue culture surfaces or PFVH-CH-B scaffold [12], suggesting that in the present study the differences in adhesion and proliferation may be influenced by surface characteristics rather than by the chemical nature of the scaffold. In agreement with these results, we and other groups have demonstrated that the topography of the substratum may influence cell attachment, proliferation and commitment [5, 18, 31-33]. Moreover, surface characteristic influences also cell spreading and cytoskeleton rearrangement which in turn could influence the differentiation potential of BMPC [31, 33-34].

In addition, we observed the BMPC growing on the surfaces of nanostructured scaffolds (SN300) by SEM (Figure 4B). In this figure it can be observed that BMPC were

able to attach and spread onto the nanostructured surfaces. The analysis of the SEM images also demonstrated that BMPC developed lamellipodia that interact tightly with the nanorods (Fig 4B, arrowheads). In this sense, previous reports have been associated the right cytoskeleton protein assembly with proper matrix-cell interactions, which in turn activates the intracellular pathways needed for osteoblastic cell growth and differentiation [33-37]. On the contrary, it has been proposed that round cell morphology caused by impairing cell adhesion complexes could modulate cell commitment against osteoblastic phenotype [34].

Then, we evaluated osteoblastic differentiation markers, namely: alkaline phosphatase activity (ALP), mineral nodules and type I collagen production. The evaluation of these differentiation markers was performed without osteogenic media (0 days of differentiation), this condition allowed us the evaluation of the direct influence of nanostructuration on osteoblastic commitment. BMPC were also incubated in the presence of osteogenic media during 15 and 21 days of culture. We found no differences on the osteoblastic markers evaluated in BMPC cultured without osteogenic media (0 days) either on plastic or scaffolds (NS170 and NS300, Figure 4C-E). However, ALP showed a significant increase after 15 days of osteoblastic differentiation ($p<0.01$), while decreases after 21 days (Figure 4C). On the contrary, mineral nodules and collagen production continued steadily increasing its levels during all the period of time studied (Figure 4D and E). Similar results were previously reported about the behavior of stem cell under osteogenic differentiation [38]. These authors associated this sequence of marker expression toward the progress of differentiation. Similarly, we could assign our results to the temporal degree of osteoblastic maturation. Moreover, in the NS300 scaffold, we found a significant increase on alkaline phosphatase activity ($p<0.01$) and mineral nodules deposition ($p<0.01$) compared to tissue culture dishes surface (plastic) at 15 or 21 days of differentiation, respectively (Figure 4C and D). These

results are in agreement with those previously published where we demonstrated that PFVH-CH-B improved osteoblastic differentiation [12]. Although this steadily increase on collagen production, in the present study we found that collagen deposition was significantly lower on all the nanostructured PFVH-CH-B surfaces studied than on control ($p<0.001$). This result could be explained by the fact that the nanostructuration of the surface also influence the extracellular matrix deposition. In this sense, we and other researchers have previously demonstrated that collagen deposition was diminished when osteoblastic cells are cultured in fibrous-nanostructured surfaces although the underlying mechanism it is not clarified [18, 39-40].

Additionally, we also evaluated the production of the extracellular matrix of glycosamineglycan (GAG) by chondrocytes. For this purpose, chondrocytes were grown by the micromass technique on the nanostructured matrices during 15 days and stained with alcian blue. We found a significant increase on GAG production by chondrocytes growing on the nanostructured surfaces compared to the tissue culture dishes surface (plastic) ($p<0.001$), , although no differences for both the nanostructured scaffolds were found (Figure 4F).

Finally, we studied the influence of nanostructuration on the inflammatory response of the PFVH-CH-B using RAW264.7 cells, a model of monocyte/macrophages in culture. We evaluated nitric oxide (NO) and interleukin-1β (IL1β) production as a function of time of culture, and IL1β, tumor necrosis factor α (TNFα) and inducible nitric oxide synthase (iNOS) mRNA by PCR as in vitro cytotoxicity markers.

We found that macrophages growing on the nanostructured scaffolds significantly increased NO production (three-folds versus control, $p<0.01$) after 6 and 48 h of culture, while there was no differences on NO production after 72 h (Figure 5A). On the other hand, there was no increase on IL1β production on the periods of time evaluated (Figure 5B) or mRNA for different markers of inflammation (Figure 5C). Moreover, our results are in

agreement with those previously reported that showed no cytotoxic response of the biomaterial [12]. Altogether, our present results demonstrated that the nanostructuration of the biomaterial elicit no further cytotoxicity in *in vitro* studies. These results are very interesting, since there are different inflammatory responses toward the tissue engineering biomaterials that could cause pro-inflammatory cells recruitment or the encapsulation and posterior rejection of the implant [41]. On the other hand, it has been also proposed that low levels of cytokine secretion could improve angiogenesis of the scaffolds [42]. Thus, to promote tissue integration there is a tight balance in cytokine production. While low levels promote angiogenesis, high levels elicit inflammatory and immunogenic responses. Additionally, we evaluated the cytotoxicity of the components released from the scaffold, if any. To demonstrate that we incubated the scaffolds in DMEM during 2 weeks and thereafter we exposed these conditioned media to BMPC monolayer. The results of this indirect cytotoxicity assay are shown in figure 5D. As it can be seen in this figure, the MTT assay demonstrated that cells exposed to these conditioned media grew as well as cells exposed to standard culture media (DMEM) even after 72 h of exposition.

4. Conclusions

In conclusion, we obtained and characterized nanostructured scaffolds of diisopropylfumarate-vinyl acetate copolymer crosslinked with chitosan (PFVH-CH-B) by by the infiltration in AAO template methodology. Thermogravimetric analysis demonstrated that our material was thermally stable displaying an initial decomposition temperature suitable for the infiltration process. The obtained nanofibers exhibited a homogeneous morphology and showed the uniform filling of the nanocavities as was demonstrated by SEM and Raman spectroscopy, respectively.

We also demonstrated that this nanostructurated biomaterial allowed BMPC adhesion and proliferation. Moreover, cells growing on the nanostructured surface showed an elongated morphology with cellular extensions that tightly interacted with the nanorods. On the other hand, our scaffolds promoted osteo- and chodro-blastic differentiation as evaluated by different specific phenotype markers. In addition, our scaffolds presented no inflammatory response *in vitro* and we observed no influence of the selected nanofibers-diameter on cell proliferation, differentiation or cytotoxicity.

Acknowledgments

This research was partially supported by Grants from the Facultad de Ciencias Exactas, Universidad Nacional de La Plata (11/X644, UNLP), and Consejo Nacional de Investigación Científica y Tecnológica (CONICET) (PIP-0035). This work was in part supported by PICT2012-0053 of ANPCYT. MLL is Doctoral Fellow of CONICET, MSM is Investigador Adjunto of CONICET, MSC is fulltime Researcher and Professor of UNLP. MINECO (PRIBRIBAR1011-1400 and MAT2014-53437-C2-2P) from Spain is also acknowledged.

References

1. Ross, A; Lahann, J, Current trends and challenges in biointerfaces science and engineering. Annual review of chemical and biomolecular engineering 2015, 6: 161-186

2. Carrow, JK; Gaharwar, AK, Bioinspired polymeric nanocomposites for regenerative medicine. Macromolecular Chemistry and Physics 2015, 216 (3): 248-264

3. Beachley, V; Wen, X, Polymer nanofibrous structures: Fabrication, biofunctionalization, and cell interactions. Prog Polym Sci 2010, 35 (7): 868-892

4. Deng, M; James, R; Laurencin, CT; Kumbar, SG, Nanostructured polymeric scaffolds for orthopaedic regenerative engineering. IEEE Trans Nanobioscience 2012, 11 (1): 3-14

5. Fernandez, JM; Cortizo, MS; Cortizo, AM; Abraham, GA, Osteoblast Behavior on Novel Porous Polymeric Scaffolds. Journal of Biomaterials and Tissue Engineering 2011, 1 (1): 86-92

6. Mijangos, C; Hernández, R; Martín, J, A review on the progress of polymer nanostructures with modulated morphologies and properties, using nanoporous AAO templates. Progress in Polymer Science 2016, 54–55: 148-182

7. Grimm, S; Martín, J; Rodriguez, G; Fernández-Gutierrez, M; Mathwig, K; Wehrspohn, RB; Gösele, U; San Roman, J; Mijangos, C; Steinhart, M, Cellular interactions of biodegradable nanorod arrays prepared by nondestructive extraction from nanoporous alumina. Journal of Materials Chemistry 2010, 20 (16): 3171-3177

8. Zhang, Z-G; Li, Z-H; Mao, X-Z; Wang, W-C, Advances in bone repair with nanobiomaterials: mini-review. Cytotechnology 2011, 63 (5): 437-443

9. Cao, H; McHugh, K; Chew, SY; Anderson, JM, The topographical effect of electrospun nanofibrous scaffolds on the in vivo and in vitro foreign body reaction. J Biomed Mater Res A 2010, 93 (3): 1151-1159

10. Cortizo, AM; Ruderman, G; Correa, G; Mogilner, IG; Tolosa, EJ, Effect of Surface Topography of Collagen Scaffolds on Cytotoxicity and Osteoblast Differentiation. J Biomater Tissue Engineer 2012, 2: 1-8

11. Cortizo, AM; Ruderman, G; Mazzini, FN; Molinuevo, MS; Mogilner, IG, Novel Vanadium-Loaded Ordered Collagen Scaffold Promotes Osteochondral Differentiation of Bone Marrow Progenitor Cells. Int J Biomater 2016, 2016: 1486350

12. Lastra, ML; Molinuevo, MS; Cortizo, AM; Cortizo, MS, Fumarate Copolymer-Chitosan Cross-Linked Scaffold Directed to Osteochondrogenic Tissue Engineering. Macromol Biosci 2017, 17 (5):

13. Martin, J; Vazquez, M; Hernandez-Velez, M; Mijangos, C, Ordered arrays of magnetic polymer-based nanorods by template synthesis. J Nanosci Nanotechnol 2009, 9 (10): 5898-5902

14. Blaszczyk-Lezak, I; Hernández, M; Mijangos, C, One Dimensional PMMA Nanofibers from AAO Templates. Evidence of Confinement Effects by Dielectric and Raman Analysis. Macromolecules 2013, 46 (12): 4995-5002

15. Martín, J; Maiz, J; Sacristan, J; Mijangos, C, Tailored polymer-based nanorods and nanotubes by" template synthesis": From preparation to applications. Polymer 2012, 53 (6): 1149-1166

16. Giussi, JM; Blaszczyk-Lezak, I; Allegretti, PE; Cortizo, MS; Mijangos, C, Tautomerizable styrenic copolymers confined in AAO templates. Polymer 2013, 54 (18): 5050-5057

17. Giussi, JM; Blaszczyk-Lezak, I; Cortizo, MS; Mijangos, C, In-situ polymerization of styrene in AAO nanocavities. Polymer 2013, 54 (26): 6886-6893

18. Lastra, ML; Molinuevo, MS; Giussi, JM; Allegretti, PE; Blaszczyk-Lezak, I; Mijangos, C; Cortizo, MS, Tautomerizable beta-ketonitrile copolymers for bone tissue engineering: Studies of biocompatibility and cytotoxicity. Mater Sci Eng C Mater Biol Appl 2015, 51: 256-262

19. Molinuevo, MS; Schurman, L; McCarthy, AD; Cortizo, AM; Tolosa, MJ; Gangoiti, MV; Arnol, V; Sedlinsky, C, Effect of metformin on bone marrow progenitor cell differentiation: in vivo and in vitro studies. J Bone Miner Res 2010, 25 (2): 211-221

20. Qiu, W; Murray, MM; Shortkroff, S; Lee, CR; Martin, SD; Spector, M, Outgrowth of chondrocytes from human articular cartilage explants and expression of alpha-smooth muscle actin. Wound Repair Regen 2000, 8 (5): 383-391

21. Uslu, I; Celikkan; Huseyin; Atakol, O; Aksu, ML, Preparation of PVA/Chitosan doped with boron composite fibers and their characterization. Hacettepe J Biol and Chem 2008, 36: 117 - 122

22. Oberti, TG; Alessandrini, JL; Cortizo, MS, Thermal characterization of novel p-nitrobezylacrylate-diisopropyl fumarate copolímero synthesized under microwave energy. J Therm Anal Calorim 2012, 109: 1525 - 1531

23. Bajpai, SK; Daheriya, P; Ahuja, S; Gupta, K, Water absorption and antimicrobial behavior of physically cross linked poly (vinyl alcohol)/carrageenan films loaded with minocycline. Designed Monomers and Polymers 2016, 19 (7): 630-642

24. Mitra, T; Sailakshmi, G; Gnanamani, A, Could glutaric acid (GA) replace glutaraldehyde in the preparation of biocompatible biopolymers with high mechanical and thermal properties? Journal of Chemical Sciences 2014, 126 (1): 127-140

25. Zając, A; Hanuza, J; Wandas, M; Dymińska, L, Determination of N-acetylation degree in chitosan using Raman spectroscopy. Spectrochimica Acta Part A: Molecular and Biomolecular Spectroscopy 2015, 134: 114-120

26. Gallardo, A; Spells, S; Navarro, R; Reinecke, H, Confocal Raman microscopy: how to correct depth profiles considering diffraction and refraction effects. Journal of Raman Spectroscopy 2007, 38 (7): 880-884

27. Ahn, J; Son, SJ; Min, J, The control of cell adhesion on a PMMA polymer surface consisting of nanopillar arrays. J Biotechnol 2013, 164 (4): 543-548

28. Cassie, ABD; Baxter, S, Wettability of porous surfaces. . Transactions of the Faraday Society 1944, 40: 546-551

29. Wenzel, RN, Resistance of solid surfaces to wetting by water. Industrial & Engineering Chemistry Research 1936, 28 (8): 988-994

30. Rasilainen, T; Suvanto, M; Pakkanen, TA, Anisotropically microstructured and micro/nanostructured polypropylene surfaces. . Surface Science 2009, 603: 2240-2247

31. Oh, S; Brammer, KS; Li, YS; Teng, D; Engler, AJ; Chien, S; Jin, S, Stem cell fate dictated solely by altered nanotube dimension. Proc Natl Acad Sci U S A 2009, 106 (7): 2130-2135

32. Park, S; Im, GI, Stem cell responses to nanotopography. J Biomed Mater Res A 2015, 103 (3): 1238-1245

33. Tsimbouri, P; Gadegaard, N; Burgess, K; White, K; Reynolds, P; Herzyk, P; Oreffo, R; Dalby, MJ, Nanotopographical effects on mesenchymal stem cell morphology and phenotype. J Cell Biochem 2014, 115 (2): 380-390

34. Biggs, MJ; Richards, RG; Gadegaard, N; Wilkinson, CD; Oreffo, RO; Dalby, MJ, The use of nanoscale topography to modulate the dynamics of adhesion formation in primary osteoblasts and ERK/MAPK signalling in STRO-1+ enriched skeletal stem cells. Biomaterials 2009, 30 (28): 5094-5103

35. Kim, DH; Provenzano, PP; Smith, CL; Levchenko, A, Matrix nanotopography as a regulator of cell function. J Cell Biol 2012, 197 (3): 351-360

36. Kim, HN; Jiao, A; Hwang, NS; Kim, MS; Kang, DH; Kim, DH; Suh, KY, Nanotopography-guided tissue engineering and regenerative medicine. Adv Drug Deliv Rev 2013, 65 (4): 536-558

37. Kim, IY; Seo, SJ; Moon, HS; Yoo, MK; Park, IY; Kim, BC; Cho, CS, Chitosan and its derivatives for tissue engineering applications. Biotechnol Adv 2008, 26 (1): 1-21

38. Malaval, L; Modrowski, D; Gupta, AK; Aubin, JE, Cellular expression of bone-related proteins during in vitro osteogenesis in rat bone marrow stromal cell cultures. Journal of Cellular Physiology 1994, 158 (3): 555-572

39. Chen, VJ; Smith, LA; Ma, PX, Bone regeneration on computer-designed nano-fibrous scaffolds. Biomaterials 2006, 27 (21): 3973-3979

40. Smith, I; Liu, X; Smith, L; Ma, P, Nanostructured polymer scaffolds for tissue engineering and regenerative medicine. Wiley Interdisciplinary Reviews: Nanomedicine and Nanobiotechnology 2009, 1 (2): 226-236

41. Padmanabhan, J; Kyriakides, TR, Nanomaterials, inflammation, and tissue engineering. Wiley Interdiscip Rev Nanomed Nanobiotechnol 2015, 7 (3): 355-370

42. Dagtekin, G; Schiffer, R; Klein, B; Jahnen-Dechent, W; Zwadlo-Klarwasser, G, Modulation of angiogenic functions in human macrophages by biomaterials. Biomaterials 2003, 24 (20): 3395-3401

Figure Legends

Scheme 1. Structure of synthesized copolymer PFVH.

Figure 1: SEM micrographs of surfaces of prepared AAO templates. (A) 3D lateral view illustrating AAO170 longitudinal (B) AAO170 and (C) AAO300 top view of AAO

Figure 2: Macroscopic aspect of the membranes (A) and SEM of free nanofibers PFVH-CH-B. B) 3D lateral view NS170; C) NS30L; D) NS170 and E) NS300 top view. CS: scaffold obtained by casting methodology.

Figure 3: Raman spectroscopy. (A) Raman spectra of PFVH-CH-B, PFVH and CH. (B) Raman spectra depth of PFVH-CH-B infiltrated in AAO 30 μm of length

Figure 4: Biocompatibility assays. (A) MTT assay (B) SEM image of a BMPC growing on the nanostructured surface. Arrowheads show the cytoplasmic cell projections that strongly interact with the biomaterial. Osteoblastic differentiation parameters: alkaline phosphatase activity (C), mineral nodules (D) and collagen type I (E). (F) GAG production. • $p<0.01$vs 2 h; •• $p<0.001$ vs. 2 h; *$p<0.01$ vs. 0 days; **$p<0.001$ vs. 0 days; # $p<0.01$ vs. plastic.

Figure 5: Cytotoxicity assay. (A) NO production. (B) IL1β (C) mRNA levels for IL1β, TNFα and iNOS. (D) Effect of the degradation products on cell viability. *$p<0.01$ vs. Plastic.

Table 1: Primer sequence for citotoxicity markers

Marker	Genbank code	Product size (bp)		Sequence
IL1β	NM_008361.3	264	fw	**AAGCTCTCCACCTCAATG**
			rv	**CAGACTCAAACTCCACTTT**
TNFα	NM_013693.3	298	fw	**CACGCTCTTCTGTCTACTG**
			rv	**CTTGAAGAGAACCTGGGA**
iNOS	NM_010927.3	499	fw	**ACCAGAGGACCCAGAGACAA**
			rv	**CGATGCACAACTGGGTGA**

Table 2. AAO Templates

	Diameter	Length
AAO_{170}	170 nm	750 nm
AAO_{300}	300 nm	750 nm
AAO^{30L}	170 nm	30 μm

Table 3. TGA data of PFVH- CHI and PFVH-CHI-B

T (°C)	PFVH- CHI	Total mass loss (%)	PFVH-CHI-B	Total mass loss (%)
IDT	263	-	242	-
T_1	280	25.3	270	16.5
T_2	323	54.1	336	43.6
T_3	457	68.8	541	59.6

IDT: initial decomposition temperatures.

Table 4. Water contact angle measurements

Sample	WCA	d (nm)*
CS	103° ± 1	-
NS170	60° ± 4	270
NS300	81° ± 2	125

* d = distance between pillars, evaluated by SEM images

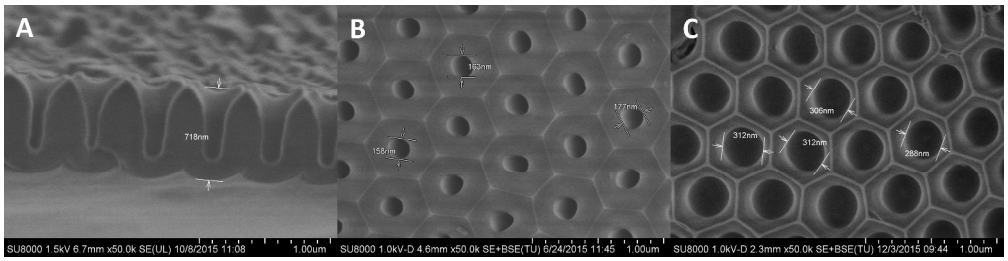

Figure 1: SEM micrographs of surfaces of prepared AAO templates. (A) 3D lateral view illustrating AAO170 longitudinal (B) AAO170 and (C) AAO300 top view of AAO

381x95mm (300 x 300 DPI)

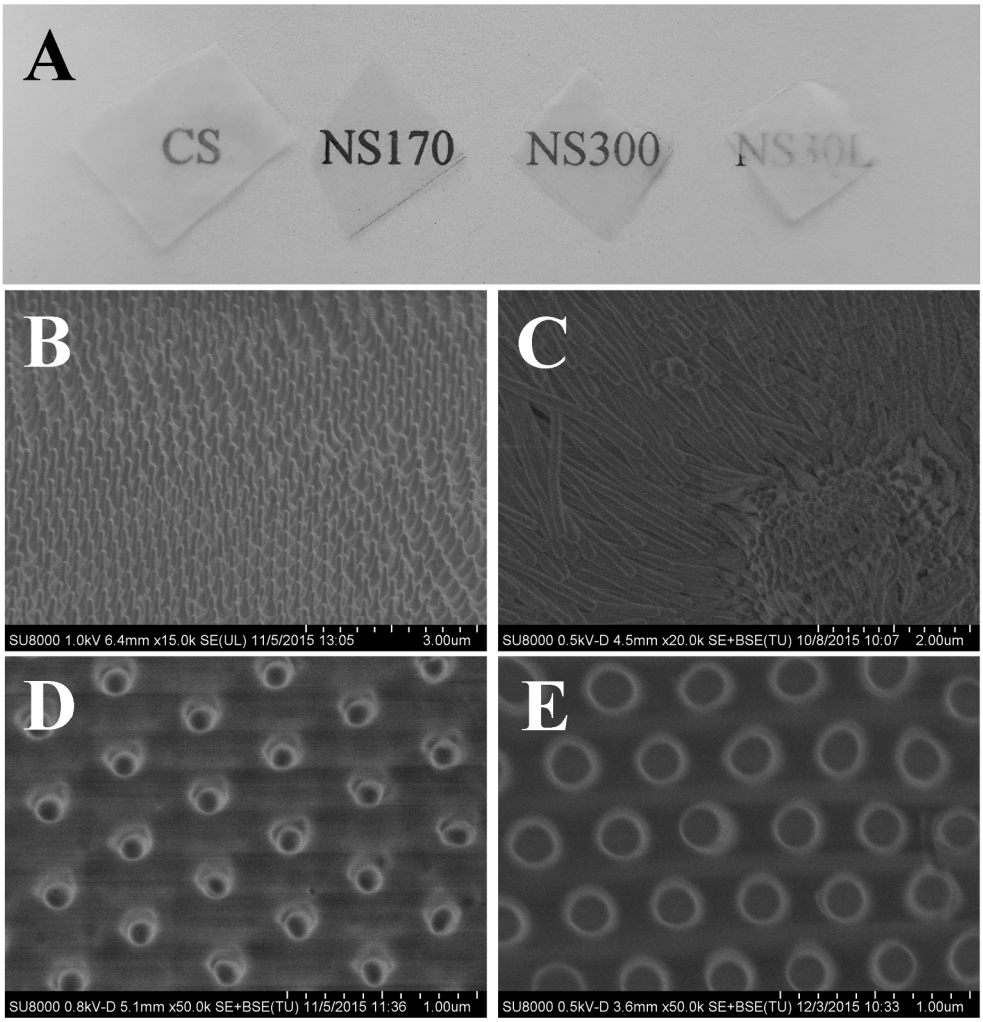

Figure 2: Macroscopic aspect of the membranes (A) and SEM of free nanofibers PFVH-CH-B. B) 3D lateral view NS170; C) NS30L; D) NS170 and E) NS300 top view. CS: scaffold obtained by casting methodology.

203x207mm (300 x 300 DPI)

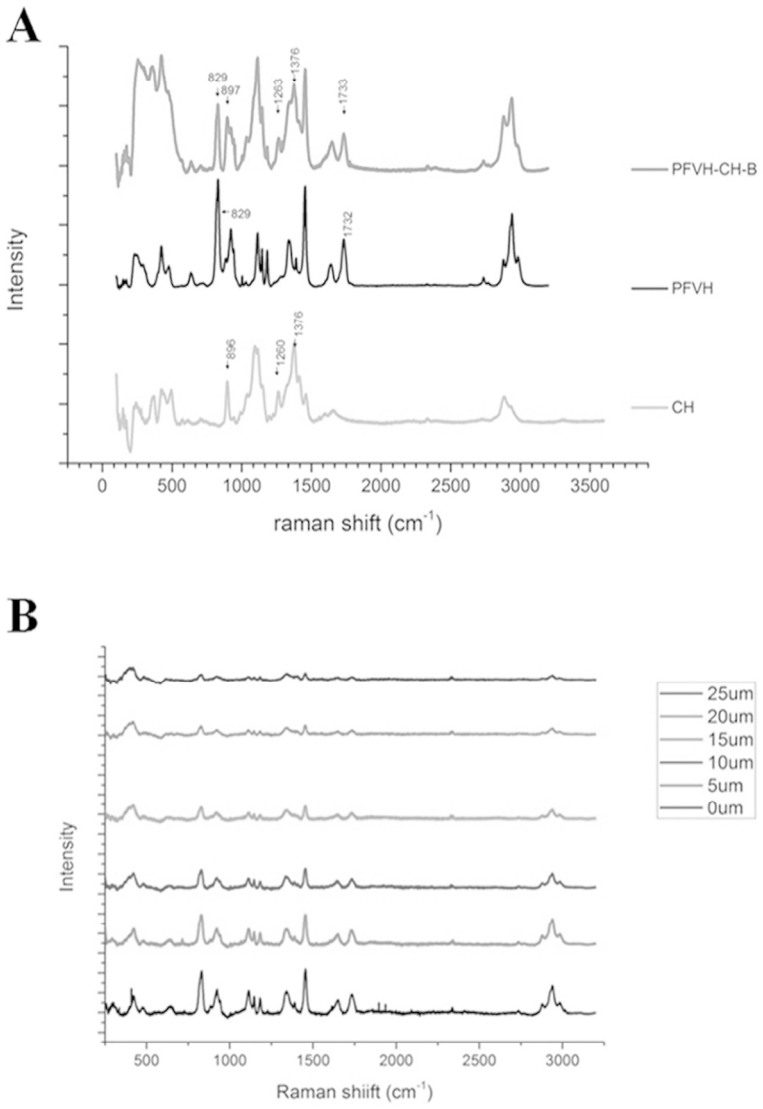

Figure 3: Raman spectroscopy. (A) Raman spectra of PFVH-CH-B, PFVH and CH. (B) Raman spectra depth of PFVH-CH-B infiltrated in AAO 30 μm of length

119x171mm (300 x 300 DPI)

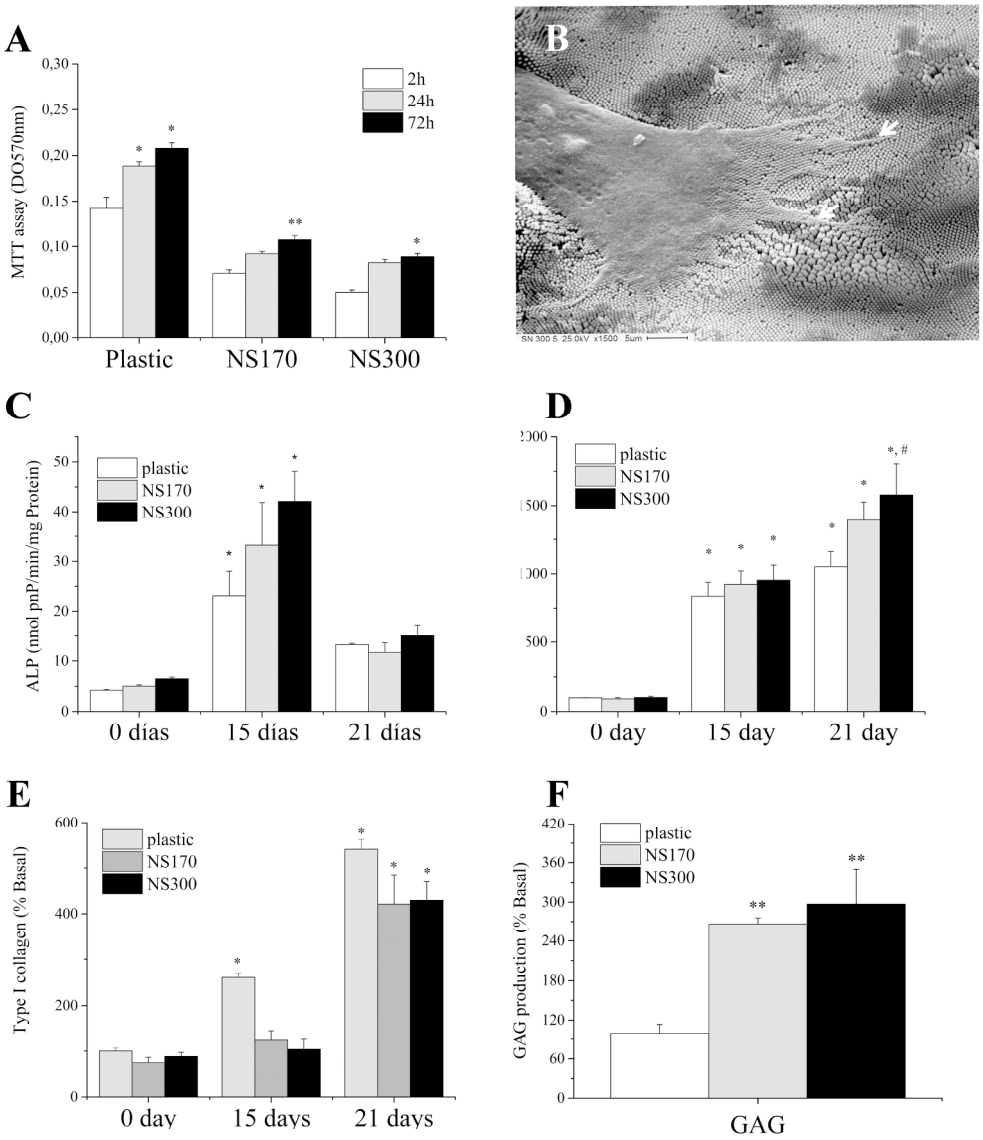

Figure 4: Biocompatibility assays. (A) MTT assay (B) SEM image of a BMPC growing on the nanostructured surface. Arrowheads show the cytoplasmic cell projections that strongly interact with the biomaterial. Osteoblastic differentiation parameters: alkaline phosphatase activity (C), mineral nodules (D) and collagen type I (E). (F) GAG production. • p<0.01vs 2 h; •• p<0.001 vs. 2 h; *p<0.01 vs. 0 days; **p<0.001 vs. 0 days; # p<0.01 vs. plastic.

230x261mm (300 x 300 DPI)

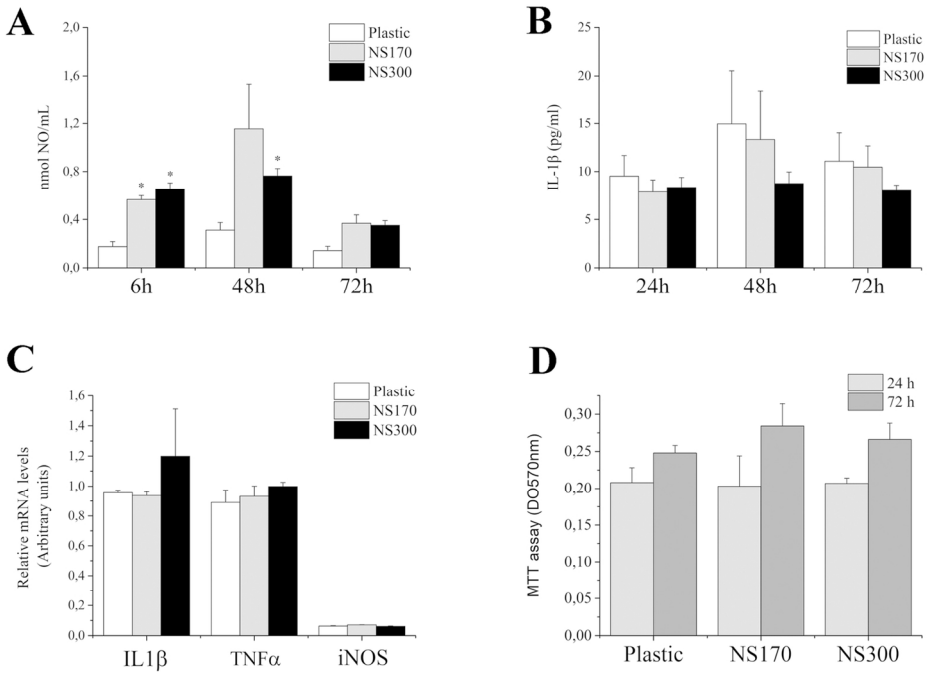

Figure 5: Cytotoxicity assay. (A) NO production. (B) IL1β (C) mRNA levels for IL1β, TNFα and iNOS. (D) Effect of the degradation products on cell viability. *p<0.01 vs. Plastic.

142x100mm (300 x 300 DPI)

Scheme 1. Structure of synthesized copolymer PFVH.

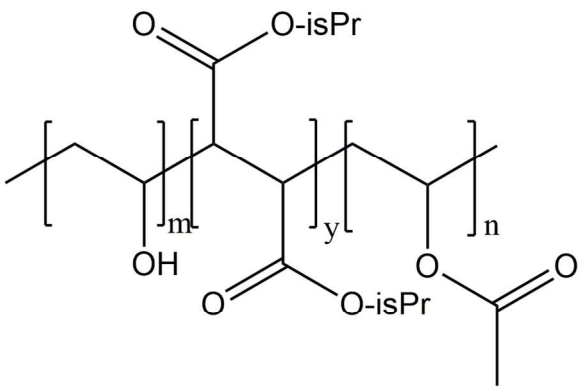

PFVH